A Novel Transceiver Design in Wideband Massive MIMO for Beam Squint Minimization

Liza Afeef, Abuu B. Kihero, and Hüseyin Arslan, *Fellow, IEEE*

***Abstract*— When using ultra-wideband signaling on massive multiple-input multiple-output (mMIMO) systems, the electromagnetic wave incurs an extra delay (across the array elements) comparable to or larger than the symbol duration, which translates into a shift in beam direction known as the beam squint effect. The beam squinting problem degrades the array gain and reduces the system capacity. This paper proposes a novel transceiver design based on lens antenna subarray and analog subband filters to compensate for the beam squinting effect. Specifically, the proposed design chunks the wideband signal from the phase shifters into groups of narrowband signals and controls their squints through an exhaustive search-based switching/precoding mechanism under the lenses. Furthermore, a simplified, thresholded search-based precoding algorithm is proposed, which demonstrates good performance while significantly minimizing complexity. The proposed system is analyzed in terms of beam gain, complexity, power consumption, and capacity. The numerical results demonstrate significant performance enhancement for the proposed system design as compared to the conventional mMIMO system with an uncompensated beam squinting problem.**

***Index Terms*— Beam squint effect, beam gain, lens antenna subarray (LAS), massive MIMO, analog subband filter, ultra-wideband (UWB) transmission.**

I. Introduction

MASSIVE multiple-input multiple-output (mMIMO) and ultra wideband (UWB) transmission have been considered among the candidate technological enablers for enhancing the performance and efficiency of the next-generation wireless networks [1], [2]. mMIMO can improve spectrum and energy efficiency, combat small-scale fading through channel hardening, and extend network coverage by overcoming the path loss (PL) problem [3]. UWB transmission not only facilitates high data rate communication but also provides resilience against multipath fading and covertness against jamming attacks [4]. Advantages of both mMIMO and UWB also span to the radio-frequency (RF) sensing aspect of the wireless networks that have been recently considered under the joint radar and communication (JRC) framework [5]. They, respectively, provide fine spatial and temporal multipath resolution, thereby facilitating accurate localization and ranging of the target objects.

Despite these desirable advantages, it has been shown that mMIMO systems implementing UWB signaling suffer from *spatial-wideband effect*, recapitulated hereunder. The Huygens-Fresnel wave propagation principle dictates that, in the antenna array systems, unless the incident signal is perpendicular to the array, the received signal at different array elements is a slightly delayed version of the original signal. The amount of delay incurred across the elements depends on the inter-element spacing and the signal's angle of arrival (AoA)/angle of departure (AoD). For a system with a relatively small number of antennas, as it is in the conventional small-scale multiple-input multiple-output (MIMO) systems, the maximum delay across the antenna aperture can be much smaller than the symbol duration, and thus its effect can be ignored. However, with high-dimensional antenna arrays, i.e., mMIMO, and with UWB signaling, this delay can be in the order or even larger than the symbol duration, leading to *delay squinting effect* in the spatial-delay domain, i.e., significant delay spread is observed across the array even in the pure line-of-sight (LoS) propagation condition. The delay squinting problem renders the steering vector frequency-dependent in the angular-frequency domain. That is, in multicarrier systems like orthogonal frequency division multiplexing (OFDM), signals at different subcarriers will point to different physical directions. Signals pertained to such derailed subcarriers might not arrive at the intended receiver or align with sidelobes or nulls of the receiver's radiation pattern, thereby degrading the performance. This phenomenon is referred to as *beam squinting* [6], [7].

A. Prior Works

Initial investigation of the beam squint effect can be found in the literature on radar technology, as large antenna array systems have been deployed there ever since [8], [9], [10], [11]. In wireless communication networks, the beam squint problem came into prominence just recently following the introduction of the mMIMO and UWB transceiver concepts. Nevertheless, several studies have already been dedicated to tackling the beam squinting problem in wireless systems.

The proposed approaches can be roughly categorized into two groups: the digital domain and analog domain based

Manuscript received 29 May 2023; revised 9 December 2023; accepted 24 February 2024. Date of publication 1 March 2024; date of current version 19 July 2024. This work was supported in part by the U.S. National Science Foundation under Award ECCS-1923857. The associate editor coordinating the review of this article and approving it for publication was J. M. Jornet. *(Corresponding author: Liza Afeef.)*

The authors are with the Department of Electrical and Electronics Engineering, Istanbul Medipol University, 34810 Istanbul, Turkey (e-mail: liza.shehab@std.medipol.edu.tr; abuu.kihero@std.medipol.edu.tr; huseyinarslan@medipol.edu.tr).

Color versions of one or more figures in this article are available at https://doi.org/10.1109/TCOMM.2024.3372885.

Digital Object Identifier 10.1109/TCOMM.2024.3372885

beam squint minimization approaches. The ideal and straightforward way of dealing with the beam squint problem in the digital domain is by designing a compensation matrix for each subcarrier that eliminates the squint-inducing phase term introduced by the spatial-wideband effect. However, this is deemed impractical as the dimension of the required compensation matrix is prohibitively large [12]. Accordingly, digital domain-based hybrid precoding approaches have been proposed in several studies [12], [13], [14], [15], [16], [17], [18], [19]. Specifically, the digital precoder is divided into two phases: performing a conventional digital precoding process for each subcarrier and then compensating for the phase drifting caused by each frequency-dependent analog precoder. Some authors have opted for radically different approaches to tackle the problem such as the works in [20] and [21]. Although they provided some promising results by approaching the problem from a codebook design perspective, complexity issues, stemming from hardware requirements or prohibitively large codebook sizes seem to haunt the proposed approaches. For example, authors of [22] proposed an Alamouti-based beamforming scheme that minimizes beam gain variation of all subcarriers within the operational bandwidth. Since the proposed beam pattern optimization involves Eigenvalues and Eigenvalues vectors computation, the computational complexity of this scheme grows with the number of antennas. In a nutshell, the digital precoding-based solutions may only offer minimal beam gain improvement while exacerbating system complexity owing to the fact that the beam squint phenomenon originates from the analog domain of the beamforming process.

The analog domain-based beam squint minimization approaches are discussed in [15], [16], [23], [24], [25], [26], and [27]. In [23], [25], and [26], authors proposed an analog precoder that leverages the true-time-delay (TTD) provided by Rotman lens array to reduce the beam squint problem. The rationale behind the approach is that the TTD provided by the Rotman lens inherently circumvents the extra transition time delay across the array (which is the main cause of the squint problem as discussed above) which reduces beam squint. Reference [16] designs a sparse antenna structure where each analog output signal is controlled by two phase shifters (PSs) at each RF chain. The PS-based proposed design can adjust the phase and amplitude of the analog precoder simultaneously while avoiding the constant-amplified precoding constraint and improving the transmission rate. However, the PSs addition causes a huge power consumption which leads to an incompetent energy-efficient system. Reference [27] and its extension [24] employ both bandpass filters and extra PSs to facilitate a subband-based beam squinting compensation. The main idea behind this approach is to chunk a wideband signal into the relatively narrowband signals using a bank of bandpass filters, followed by an additional phase shift with respect to the center frequency of each filter. While the approach sounds viable, the overall analog design still faces some challenges that need to be addressed. Specifically, the adoption of an extra layer of PSs network has an obvious drawback of reducing system's energy efficiency.

B. Contributions

In order to compensate for the beam squint effect in the analog domain and enhance the system performance while maintaining an energy-efficient system without the use of extra PS network as the aforementioned works, an analog antenna design is proposed in UWB mMIMO systems. In this paper, a novel analog transceiver design is proposed based on a cooperation between a lens antenna subarray (LAS) structure and analog subband filters to minimize the beam squint problem. Generally, LAS design presented in [28], [29] increases the array's scan range and steering resolution compared to other subarray structures. This is due to employing two steering mechanisms using both PSs and switching networks. In addition to the aforementioned LAS design advantages, this work modifies the LAS structure that leverages the combination of the two steering mechanisms to compensate for the beam squint problem. Specifically, different from the conventional LAS design, a bank of analog subband filters is introduced between PSs and the switching elements under the lenses to chunk the wideband signal into several subbands such that the subcarriers within a given subband lead to relatively same amount of squinting. For each subband, the switching mechanism is used to select an appropriate antenna element under each lens that can correct/minimize the deviation (i.e., squinting due to the center frequency of a given subband) of the resultant beam from the intended direction determined by the PSs.

Here it is pertinent to clarify that the proposed approach was first discussed in our preliminary works [30] and [31]. In [31], we developed a beam squint-based multiple access scheme where the proposed LAS framework was used to flexibly control the squinted beams and direct them toward different locations to serve different users. Following the promising performance obtained in [31], this work intends to provide an in-depth analysis of this approach from a beam squint minimization perspective and its associated capacity, energy efficiency, and complexity performances. We also provide a thorough comparison with the state-of-the-art beam squint minimization approaches. The main contribution of this work can be summarized as follows:

- A novel analog transceiver design based on LAS structure is presented and evaluated for mitigating the beam squinting problem in UWB mMIMO systems. Our proposed design inherits the energy-efficient nature of the LAS structure, making it more appealing not only from an affordability perspective but also for the envisioned green-communication networks, unlike the contemporary approaches presented in [24] and [27] that employ analog filters as well as extra PSs networks in their designs which significantly degrades the energy efficiency of the system.
- The proposed system is designed according to the worst-case beam squinting scenarios, i.e., considering the maximum scanning angle of the array and maximum bandwidth to be supported, such that it applies to all other cases without requiring any hardware modification.
- While the proposed design can work with the traditional exhaustive search-based precoder for antenna selection

under the lenses, an enhanced, threshold-based precoder is also proposed to reduce the search complexity without notable degradation on the beam-gain performance.
- Furthermore, the analog precoder of the proposed design can be flexibly controlled to enhance the performance without requiring any hardware replacement as it is the case with the existing works with their fixed precoders.

C. Organization and Notations

The rest of this work is organized as follows. The system model of the conventional mMIMO that leads to the beam squinting problem is recapped in Section II. Detailed explanation and analysis of the proposed LAS-based design and its proposed precoder are given in Section III, followed by the system analysis in IV. The numerical evaluation is presented in Section V. Section VI finally concludes the work.

*Notation:*Matrices are denoted by bold uppercase letters (e.g. $\mathbf{A}$), and vectors are denoted by bold lowercase letters (e.g. $\mathbf{a}$). $\mathbf{A}^T$ and $\mathbf{I}_Z$ denote the Hermitian (conjugate transpose) of matrix $\mathbf{A}$ and $Z \times Z$ identity matrix, respectively. $\odot$ represents the Hadamard product, $\mathcal{CN}(\mu, \sigma)$ stands for the complex normal distribution with mean μ and variance σ, and $\mathcal{O}(.)$ represents the standard "big O" notation. Finally, $E\{\cdot\}$ denotes the expectation operator.

II. System Model and Problem Analysis

A mMIMO system with a base station (BS) equipped with M-antennas uniform linear array (ULA) is considered. Suppose there are L_p channel paths arriving at the BS where each path $\ell \in \{1, 2, \ldots, L_p\}$ is associated with a passband complex gain α_ℓ, AoA/AoD $\hat{\theta}_\ell \in [-\pi/2, \pi/2)$, and a propagation delay $\tau_\ell \in [0, \tau_{\max}]$, where $\tau_{\max}$ is the channel's maximum delay spread. As briefly mentioned in Section I, for a mMIMO system implementing very wideband signaling, there exists a non-trivial amount of delay across the array elements (with respect to the first element), given by [7]

$$\Delta\tau_{m,\ell} = (m-1)\frac{d\sin\hat{\theta}_\ell}{c} \tag{1}$$

with c is speed of light, $d = \lambda_c/2$ being inter-element spacing where λ_c is the carrier wavelength, and $m \in \{1, 2, \ldots, M\}$. Consequently, the total delay of an ℓ^{th} path observed by m^{th} element can be given as

$$\tau_{m,\ell} = \tau_\ell + \Delta\tau_{m,\ell}. \tag{2}$$

Accordingly, the channel impulse response (CIR) observed by the m^{th} element is given as

$$h_m(t) = \sum_{\ell=1}^{L_p} \beta_\ell e^{-j2\pi f_c \tau_{m,\ell}} \delta(t - \tau_{m,\ell}), \tag{3}$$

where β is the complex path gain, f_c is the carrier frequency given as $f_c = c/\lambda_c$ where c is the speed of light.

Taking the Fourier transform of (3) and with some simplification, the channel frequency response (CFR) of the considered link is obtained as [2]

$$h_m(f) = \sum_{\ell=1}^{L_p} \tilde{\beta}_\ell e^{-j2\pi(m-1)\frac{d\sin\hat{\theta}_\ell}{\lambda_c}} \underbrace{e^{-j2\pi(m-1)\frac{fd\sin\hat{\theta}_\ell}{c}}}_{\text{squint-inducing term}} e^{-j2\pi f\tau_\ell}, \tag{4}$$

where $\tilde{\beta}_\ell = \beta_\ell e^{-j2\pi f_c \tau_\ell}$ is the equivalent baseband path gain. Stacking the channels from all M antennas, the CFR vector over the whole array can be expressed as

$$\mathbf{h}(f) = \sum_{\ell=1}^{L_p} \tilde{\beta}_\ell \underbrace{\mathbf{a}_{\text{ideal}}(\hat{\theta}_\ell) \odot \mathbf{a}_{\text{squint}}(\hat{\theta}_\ell, f)}_{=\,\mathbf{a}_{\text{eff}}}(\hat{\theta}_\ell, f) e^{-j2\pi f\tau_\ell}, \tag{5}$$

where $\mathbf{a}_{\text{ideal}}(\hat{\theta}_\ell) = [1, e^{-j2\pi\frac{d\sin\hat{\theta}_\ell}{\lambda_c}}, \ldots, e^{-j2\pi(M-1)\frac{d\sin\hat{\theta}_\ell}{\lambda_c}}]$ is the perfect spatial-domain steering vector and $\mathbf{a}_{\text{squint}}(\hat{\theta}_\ell, f) = [1, e^{-j2\pi\frac{fd\sin\hat{\theta}_\ell}{c}}, \ldots, e^{-j2\pi(M-1)\frac{fd\sin\hat{\theta}_\ell}{c}}]$ is a frequency-dependent vector that induces beam-squinting problem in the system. As such, $\mathbf{a}_{\text{squint}}$ modifies $\mathbf{a}_{\text{ideal}}$ into a frequency-dependent effective steering vector $\mathbf{a}_{\text{eff}}$

$$\mathbf{a}_{\text{eff}}(\hat{\theta}_\ell, f) = \Big[1, e^{-j2\pi(f+f_c)\frac{d\sin\hat{\theta}_\ell}{c}}, \cdots, e^{-j2\pi(M-1)(f+f_c)\frac{d\sin\hat{\theta}_\ell}{c}}\Big]^T. \tag{6}$$

Based on the array response $\mathbf{a}_{\text{eff}}(\theta, f)$ and a pre-designed beamforming vector $\boldsymbol{w} = \mathbf{a}_{\text{ideal}}(\hat{\theta})$, the beam gain function is give by

$$\begin{aligned} g^{(\text{BS})}(\theta, f) &= \frac{1}{\sqrt{M}} \boldsymbol{w}^H \mathbf{a}_{\text{eff}}(\theta, f), \\ &= \frac{1}{\sqrt{M}} \sum_{m=1}^{M} e^{-j2\pi\frac{d}{c}(m-1)\left[(f+f_c)\sin\theta - f_c\sin\hat{\theta}\right]}. \end{aligned} \tag{7}$$

Assuming that $x(\theta, f) = \frac{d}{c}[(f + f_c)\sin\theta - f_c\sin\hat{\theta}]$, the beam gain can be written as

$$g^{(\text{BS})}(\theta, f) = \frac{1}{\sqrt{M}} \frac{\sin(\pi x(\theta, f)M)}{\sin(\pi x(\theta, f))} e^{-j\pi x(\theta,f)(M-1)}. \tag{8}$$

In multicarrier signaling, $\mathbf{a}_{\text{eff}}$, being frequency-dependent, directs signal pertaining to different subcarriers to different directions away from the desired direction. From (5), the effective direction of the signal at subcarrier k centered at $f_k = ((k-1) - (N-1)/2) \times \Delta f + f_c$, where $k = 1, 2, \cdots, N$ with N and Δf being the fast Fourier transform (FFT) size and subcarrier spacing, respectively, can be found as [20] and [32]

$$\theta(f_k) = \sin^{-1}\left(\frac{\sin\hat{\theta}}{1 + \frac{f_k - f_c}{f_c}}\right), \tag{9}$$

which does not align with the desired direction. The amount of incurred beam deviation due to k^{th} subcarrier can be given as

$$\Delta\theta(f_k) = |\hat{\theta} - \theta(f_k)|. \tag{10}$$

Likewise, the beam loss (BL) in the desired direction due to squinting caused by k^{th} subcarrier can be quantified by

$$\text{BL}(f_k) = \left.\frac{g(\hat{\theta}) - g^{(\text{BS})}(\hat{\theta}, f)}{g(\hat{\theta})}\right|_{f=f_k-f_c}, \tag{11}$$

where $g(\hat{\theta}) = g^{(\text{BS})}(\hat{\theta}, f)|_{f=f_k-f_c}$ and $f_k = f_c$ is the ideal beam gain in the desired direction in the absence of beam squinting which is equal to $\sqrt{M}$. This beam loss directly translates into the system capacity degradation. For a system

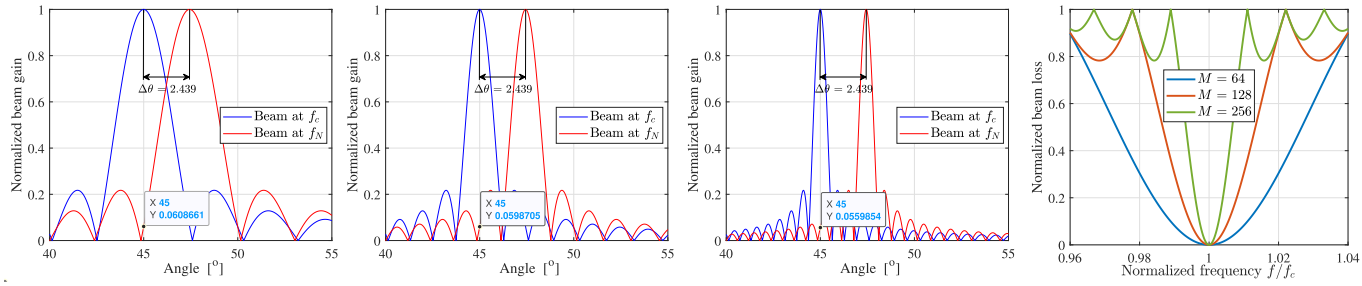

(a) $M = 64$ (b) $M = 128$ (c) $M = 256$ (d) Beam loss analysis.

Fig. 1. Normalized beam gain vs beam angle analysis at different antenna array size with $f_c = 60$ GHz.

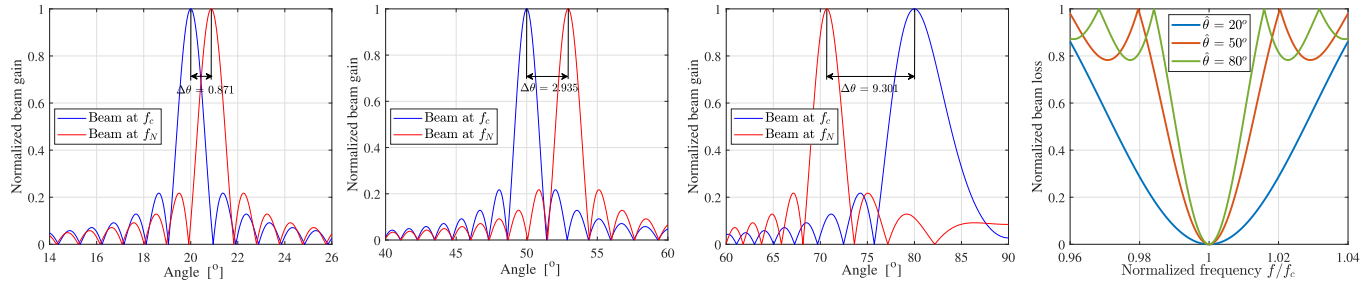

(a) $\hat{\theta} = 20^o$ (b) $\hat{\theta} = 50^o$ (c) $\hat{\theta} = 80^o$ (d) Beam loss analysis.

Fig. 2. Normalized beam gain vs beam angle analysis at different beam direction with $f_c = 60$ GHz.

with N_{RF} RF chains operating with bandwidth W under LoS channel and signal-to-noise ratio (SNR) γ, the system capacity is given by

$$C_{\text{TA}} = \frac{W}{N} \sum_{r=1}^{N_{\text{RF}}} \sum_{k=1}^{N} \log_2 \left[1 + \frac{\gamma}{N_{\text{RF}} \frac{W}{N}} |g^{(\text{BS})}(\hat{\theta}_r, f_{k,r})|^2 \right]. \tag{12}$$

From the above analysis, it can be deduced that the effect of beam squint on the system performance is determined by three main factors: the number of antenna elements M, system bandwidth with respect to the operating frequency W/f_c, and the desired beam direction $\hat{\theta}$. Figs. 1—3 illustrate the impacts of these factors on the beam directions across the subcarriers and the consequent beam loss. For clarity, only beams due to the middle subcarriers ($f_k = f_c$) and the furthest subcarrier ($f_k = f_N$) are plotted.

Figs. 1a—1c show that as the array size increases the maximum beam deviation from the desired direction remains the same. However, since the beams become narrower with large array sizes, the squinted beams tend to split from each other. The narrow squinted beams contribute less gain toward the desired direction as most of their energy is focused toward the squinted direction. This leads to higher beam loss as depicted in Fig. 1d. Therefore, larger array dimensions worsen the effect of the beam squint phenomenon on the system performance.

In Figs. 2a—2c, the impact of the $\hat{\theta}$ is illustrated. It is clear that the squinting phenomenon intensifies as the desired direction $\hat{\theta}$ deviates from the array's boresight. Fig. 2a shows that when $\hat{\theta}$ aligns with arrays boresight (i.e., $\hat{\theta} = 0$) no squinting effect is observed regardless of the array size and the used bandwidth. However, as the $\hat{\theta}$ deviates to the right or left of the array's boresight, beam squint comes into the picture and its effect increases as $\hat{\theta}$ increases, as illustrated by Figs. 2b and 2c. Consequently, the beam loss also grows with $\hat{\theta}$ as shown in Fig. 2d.

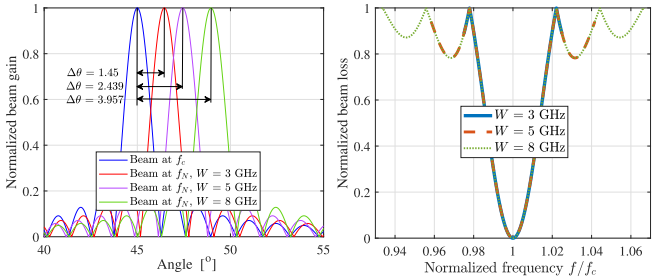

(a) (b)

Fig. 3. Normalized beam gain vs beam angle analysis at different fractional bandwidth with $f_c = 60$ GHz.

Fig. 3 shows the effect of bandwidth W on the beam squint. The analysis is done for $W = 3$ GHz, 5 GHz, and 8 GHz. As the bandwidth increases, edge subcarriers incur more frequency deviations from the carrier frequency f_c. This causes them to incur a larger squinting effect as well as more beam loss which directly degrades the system's throughput.

Since the use of massive antenna arrays and UWB signaling is inevitable in the future wireless system, techniques to deal with the beam squint problem are highly necessary in order to ensure reliable performances in these systems. The transceiver design presented in the subsequent section is dedicated to minimizing the squinting problem taking the complexity and energy efficiency issues into account.

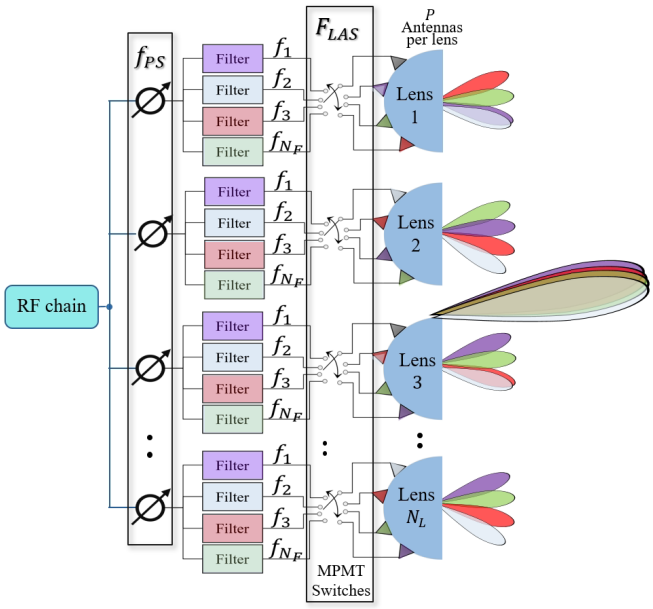

Fig. 4. The proposed LAS analog transceiver design for a multicarrier signal in mMIMO systems.

III. The Proposed LAS-Based System Design

In this section, the proposed transceiver design alongside its novel analog domain precoding technique to minimize the beam squint effect are discussed.

A. Proposed Transceiver Design

This work leverages the unique design of the LAS transceiver presented in our earlier work [28] that gives the inherent ability to control the signal in the analog domain.

The conventional LAS design consists of N_L discrete lenses with P antenna elements connected to the focal surface of each lens. The total number of antenna elements under all lenses is equal M, placed in a way that the resultant antenna gain of the array is similar to half-wave spaced M antenna elements set in a ULA. The lenses are connected to the PS network by single pole multiple throw (SPMT) switches. One antenna element is activated under each lens by controlling the SPMT switching network to provide a sub-beam with a specific direction and low gain. As a result, one narrower beam with higher beamforming gain is produced for transmission from the combination of these sub-beams which is approximately equal to the beam generated by a half-wave spaced M antenna elements placed in a ULA.

In this work, a modified LAS structure is proposed to specifically account for the beam squinting effect. The modified design features analog subband filters inserted between the PSs and the switching elements. The role of these filters is to chunk the wideband signal into groups of narrowband signals such that the subcarriers within each group experience a relatively similar amount of squinting. It also features the multiple pole multiple throw (MPMT) instead of the SPMT switching network for relaying all the narrowband groups to their respective antennas elements (based on the degree of their squinting) under the lenses, as shown in Fig. 4.

At the transmitter, at each RF chain, the UWB signal passes through the PS network where each PS adds a fixed delay to the incoming RF signal based on the desired direction $\hat{\theta}$.[1] As such, the PS precoder design is determined by $\mathbf{a}_{\text{ideal}}$ and can be given as

$$\mathbf{f}_{\text{PS}} = \frac{1}{\sqrt{N_L}} \left[1, e^{j\frac{2\pi d_L}{\lambda_c}\sin\hat{\theta}}, \cdots, e^{j\frac{2\pi d_L}{\lambda_c}(N_L-1)\sin\hat{\theta}}\right]^T, \quad (13)$$

where d_L is the distance between the lenses assumed to be $d_L = P \times d$. The output of each PS is then passed through N_L groups of analog subband filters (each group has N_F parallel analog subband filters) to chunk the wideband signal into N_F narrowband signals of bandwidth W_b where $W_b = W/N_F$ and W is the system bandwidth. N_F is decided based on the amount of squint that the system can tolerate.

The extreme case for the design is to compensate the squint due to each individual subcarrier, which would require $N_L \times N$ filters for the whole design. To relax the design requirement, it is assumed that the squinting within the quarter of 3 dB beamwidth $\Omega_{3\text{dB}}$ is tolerable inside each subband, i.e.,

$$\left|\theta(f_{k_{\text{edge}}}) - \theta(f_{k'})\right| \leq \frac{\Omega_{3\text{dB}}}{8}, \quad (14)$$

where $\Omega_{3\text{dB}} \approx (0.89\lambda)/(Md)$ for ULA [33], $f_{k'} = ((k'-1) - (N_F-1)/2)\,\Delta f + f_c$ is the center frequency of the filter, with $k' = 1, 2, \cdots, N_F$, and $f_{k_{\text{edge}}} = f_{k'} \pm W_b/2$ is the carrier frequency of a subcarrier at the edge of k'-th subband (see Fig. 5).

Using (9), (14) can be simplified to

$$\left|\sin^{-1}\left(\frac{\sin\hat{\theta}}{1+\frac{\Delta f}{2f_c}(2k'-N_F-\frac{N}{N_F}-1)}\right) - \sin^{-1}\left(\frac{\sin\hat{\theta}}{1+\frac{\Delta f}{2f_c}(2k'-N_F-1)}\right)\right| \leq \frac{\Omega_{3\text{dB}}}{8}, \quad \text{s.t. } N \mod N_F = 0. \quad (15)$$

For simplicity, we consider the subband centered at f_c such that $f_{k'} = f_c$ and $k' = (N_F+1)/2$. Consequently, (15) reduces to

$$\left|\hat{\theta} - \sin^{-1}\left(\frac{\sin\hat{\theta}}{1+\frac{W}{2f_c N_F}}\right)\right| \leq \frac{\Omega_{3\text{dB}}}{8}, \quad \text{s.t. } N \mod N_F = 0. \quad (16)$$

Considering that the severity of the beam squint increases as $\hat{\theta}$ grows (equation (1)), N_F is optimized based on the maximum scanning angle of the LAS system (i.e., $\hat{\theta} = \pi/4$ [28]) such

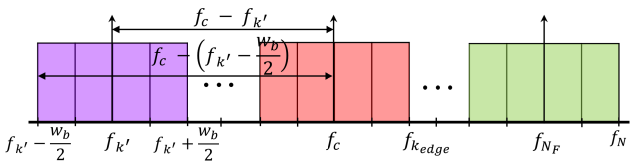

Fig. 5. Sub-grouping the subcarriers in the subband filters.

[1]Note that the multipath index ℓ is dropped here and in the subsequent equations just for the sake of notational simplicity.

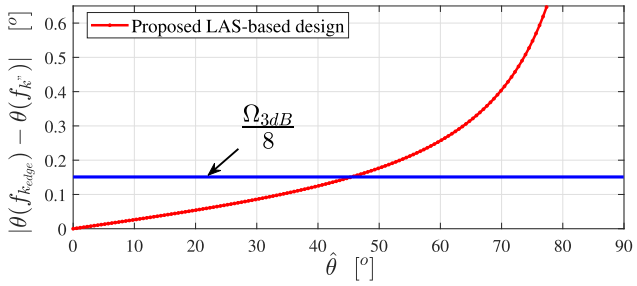

Fig. 6. Squinting amount of a given subband for any desired direction within LAS's scanning range is within the tolerable range ($\Omega_{3\text{dB}}/8$). Here, (17) is used to calculate N_F, with $W = 5$ GHz and $f_c = 60$ GHz.

that it is applicable for all users within the scanning range (See Fig. 6). This leads to

$$N_F \geq \frac{W \sin(\pi/4 - \Omega_{3\text{dB}}/8)}{\sqrt{2} f_c (1 - \sqrt{2}\sin(\pi/4 - \Omega_{3\text{dB}}/8))}. \tag{17}$$

Here it is pertinent to mention that W in (17) should be the maximum bandwidth to be supported by the system such that the designed N_F is also applicable for arbitrary signal bandwidths below W. Note that when the signal bandwidth is less than the specified maximum bandwidth, some subbands (edge subbands in particular) may be turned off as they may contain no subcarrier.

Each narrowband signal passes through the switching mechanism using MPMT switches is modeled by a precoder F_{LAS} to the lenses for transmission. The MPMT switches allow simultaneous activation of N_F (one for each subband) antennas under each lens. For the n^{th} lens (where $n = 0, 1, \cdots, N_L - 1$), the switching mechanism is represented by a selection vector $\mathbf{s}^{(n)} \in B^{P\times 1}$. If an antenna element is activated, its location in the selection vector is represented by logic 1. The activated p-th antenna element produces a beam at direction $\theta^{(n)}(p) = \frac{\pi}{4} - \frac{p}{(P-1)}\frac{\pi}{2}$, where P is the total number of antenna elements under each lens and $p = 0, 1, \ldots, P-1$ as explained in [28]. On the other hand, the inactivated elements' locations are represented by logic 0 in the selection vector $\mathbf{s}^{(n)}$. Therefore, the switch precoder matrix $\mathbf{F}_{\text{LAS}}$ is given as

$$\mathbf{F}_{\text{LAS}} = \begin{bmatrix} \mathbf{s}^{(0)} & \mathbf{0} & \cdots & \mathbf{0} \\ \mathbf{0} & \mathbf{s}^{(1)} & & \mathbf{0} \\ \vdots & & \ddots & \vdots \\ \mathbf{0} & \mathbf{0} & \cdots & \mathbf{s}^{(N_L-1)} \end{bmatrix}, \tag{18}$$

where $\mathbf{0}$ is a vector of size $P\times 1$ with all elements set to zeros. Note that the zeros in the $\mathbf{F}_{\text{LAS}}$ matrix indicate that there is no contribution between subarrays to the individual beams that they generate. For the k'-th subband filter, one antenna element is activated under each lens.

Since the lens generates a beam toward a specific direction based on the selected antenna to be activated under it, the binary selection vector $\mathbf{s}^{(n)}$ can be equivalent to [28]

$$\mathbf{s}^{(n)} = \frac{1}{\sqrt{P}}\Big[e^{-j2\pi\frac{d}{c}f_c\frac{P-1}{2}\sin\theta^{(n)}}, \cdots, 1, \cdots, e^{-j2\pi\frac{d}{c}f_c\frac{-(P-1)}{2}\sin\theta^{(n)}}\Big]^T. \tag{19}$$

Eventually, the effective RF precoder, $\mathbf{f}_{\text{RF}}$, for the proposed design is given as

$$\mathbf{f}_{\text{RF}} = \mathbf{F}_{\text{LAS}}\mathbf{f}_{\text{PS}}, = \frac{1}{\sqrt{N_L}}\begin{bmatrix} 1\times\mathbf{s}^{(0)} \\ e^{j2\pi\frac{d}{c}Pf_c\sin\hat{\theta}}\times\mathbf{s}^{(1)} \\ \vdots \\ e^{j2\pi\frac{d}{c}Pf_c(N_L-1)\sin\hat{\theta}}\times\mathbf{s}^{(N_L-1)} \end{bmatrix}. \tag{20}$$

Therefore, the $(Pn+p)$-th element in $\mathbf{f}_{\text{RF}}$ vector is given as

$$\{\mathbf{f}_{\text{RF}}\}_{(Pn+p)} = \frac{1}{\sqrt{N_L P}} e^{j2\pi\frac{d}{\lambda_c}Pn\sin\hat{\theta}} e^{-j2\pi\frac{d}{\lambda_c}(\frac{(P-1)}{2}-p)\sin\theta^{(n)}}. \tag{21}$$

Let $\theta_{LAS}(k')$ be the k'-th subband's effective beam direction given by the proposed LAS design with arbitrary values of $\theta^{(n)}$'s across the lenses, then the maximum beam gain $g_{\max}$ of the design at k'-th subband is obtained as

$$\begin{aligned} g_{\max}(\theta_{\text{LAS}}(k'), f_{k'}) &= \mathbf{f}_{\text{RF}}^H\ \mathbf{a}_{\text{eff}}(\theta_{\text{LAS}}(k'), f_{k'}), \\ &= \frac{1}{\sqrt{N_L P}}\sum_{n=0}^{N_L-1}\sum_{p=0}^{P-1} e^{-j2\pi\frac{d}{c}(Pn+p)(f_{k'}+f_c)\sin\theta_{\text{LAS}}(k')} \\ &\quad\times e^{-j2\pi\frac{d}{c}f_cPn\sin\hat{\theta}} e^{-j2\pi\frac{d}{c}f_c(\frac{(P-1)}{2}-p)\sin\theta^{(n)}}. \end{aligned} \tag{22}$$

For each subband, the proposed design seeks to find the set $\Phi(k') = \{\theta^{(1)}, \theta^{(2)}, \ldots, \theta^{(n)}, \ldots, \theta^{(N_L)}\}$ that gives optimum $\theta_{\text{LAS}}(k')$, i.e.,

$$\theta_{\text{LAS}}^{\text{opt}}(k') = \min_{\Phi(k')} |\hat{\theta} - \theta_{\text{LAS}}(k')|. \tag{23}$$

This can be done by the exhaustive search approach whose complexity for each subband can be quantified as $\mathcal{O}\left(P^{N_L} - k' + 1\right)$. Note that increasing the number of lenses in the design achieves better angle resolution in (23) to reach exact $\hat{\theta}$ which enhances the beam gain and thus system capacity. However, this may lead to an exponential growth of the precoding complexity. Therefore, an optimum number of lenses needs to be considered in the system design that achieves acceptable angle resolution with affordable complexity overhead.

B. Proposed Threshold-Based Precoding

In order to reduce the complexity of the exhaustive search approach, a threshold-based search mechanism is proposed. In this case, a threshold is specified (based on the desired performance) to allow the selection of a sub-optimal set of antennas over the lenses for a given k'-th subband. Once the sub-optimal set that satisfies the specified threshold is found, the search process continues with the next subband. This avoids the searching over all $(P^{N_L} - k' + 1)$ possible combinations of the antenna under all lenses for a given subband, thereby reducing the complexity.

In the proposed precoder, it is assumed that, for the middle subband (i.e., $f_{k'}|_{k'=N_F/2}$) the beam deviation within a specific threshold (i.e., $\Omega_{3\text{dB}}$ of the desired beam direction) is acceptable. Since different subbands experience different amounts of squint, the threshold is scaled based on $f_{k'}$ with

Algorithm 1 The Proposed LAS Framework.

Input: f_c, W, M, $\hat{\theta}$.
Output: $\mathbf{F}_{\text{LAS}}^{(\text{opt})}$.
Calculate the optimum number of analog subband filters N_F as specified in (17).
Build the proposed LAS design as illustrated in Fig. 4.
Set the PS precoder as in (13).
Define all possible sets for $\mathbf{s}_t^{(n)}$ to build a possible $\mathbf{F}_{\text{LAS}}$.
Define the half-power beamwidth $\Omega_{3\text{dB}}$ of the design.
for $k' = N_F/2, N_F/2 \pm 1, \ldots$ **do**
  Select the initial set of searching as $\Phi_{\text{init}}(k') = \{\hat{\theta}, \hat{\theta}, \ldots, \hat{\theta}\}$.
  Calculate $\theta_{\text{LAS}}(k')$ that satisfies (22).
  while $|\hat{\theta} - \theta_{LAS}(k')| > \frac{\Omega_{3dB}}{2} \times \left(1 + \left|\frac{f_{k'} - f_c}{f_c}\right|\right)$ **do**
    Go to the next set $\Phi(k')$.
    Repeat step 8.
  Assign the sub-optimum set to the given subband and remove this set from the possible sets for the next subband.
Build $\mathbf{F}_{\text{LAS}}$ from the optimum selected sets.

respect to f_c. Hence, the search seeks to find a sub-optimal set of antennas for the k'-th subband that satisfies

$$|\hat{\theta} - \theta_{\text{LAS}}(k')| \leq \frac{\Omega_{3\text{dB}}}{2} \times \left(1 + \left|\frac{f_{k'} - f_c}{f_c}\right|\right). \quad (24)$$

Since the squint causes beam deviation from the desired direction $\hat{\theta}$, the search process for a given subband begins around $\hat{\theta}$ by setting the initial beam direction under the lenses as $\Phi_{\text{init}}(k') = \{\hat{\theta}, \hat{\theta}, \ldots, \hat{\theta}\}$. Note that each subband has a different amount of squinting, thus the combination of $\theta^{(n)}$'s that makes up the optimum set $\Phi(k')$ is unique for each subband. Therefore, such a combination can be removed from the search sets of the next subbands, thereby reducing the search complexity even further. Note that, with the $\Phi(k')$ initialization approach proposed above, the subband with the least squinting converges faster. As such, the searching process is initialized from the middle to the edge subbands to reduce the size of the search sets at the edge subbands.

The proposed LAS-based design with its precoding are summarized in Algorithm 1. Additionally, Fig. 7 provides a quick recap of how the proposed system operates. In a nutshell, for each subband, one antenna element is selected under each lens. Since the aim of the design is to minimize the beam squint for a given subband, the selected antenna combinations across the lenses should result into one best effective beam that has the minimum deviation from the desired beam direction $\hat{\theta}$. For a design with N_L lenses and P antennas under each lens, there are P^{N_L} possible ways of selecting the antennas under the lenses for each given subband. To find the best effective beam, the exhaustive search algorithm can be employed to search over all P^{N_L} possible combinations, and the one that results in the best beam is selected for a given subband. Note that, since different subbands experience

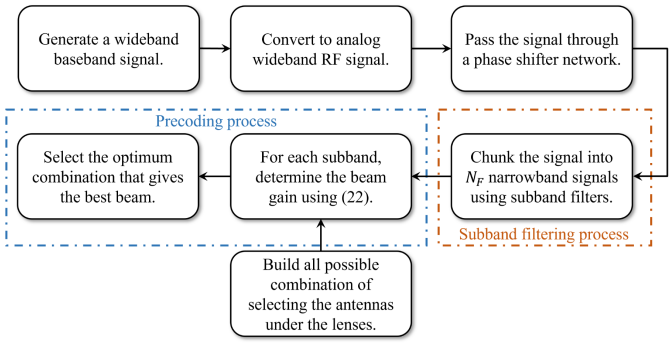

Fig. 7. The signal flow chart in the proposed LAS design.

different amounts of squinting, the optimum selected antenna combination across the lenses can differ for each subband. The beam search complexity can be reduced by employing the proposed threshold-based precoding algorithm instead of the full exhaustive search algorithm.

It is important to mention that, although the proposed design is described from the transmitter perspective, it can be also applied on the receiver side as long as the receiving node implements the mMIMO system and the beam squint problem exists.

C. Extension to Multiple Users Scenario

Considering a multi-user UWB mMIMO system in which the BS makes use of the M antennas and N_{RF} RF chains to communicate with U single-antenna users where $U \leq N_{\text{RF}}$. The system is adjusted for transmission/reception based on its own structure as follows:

- In fully-connected hybrid mMIMO designs [34], the array size under each RF chain can be considered massive, and therefore the proposed design should be implemented in each RF chain. At this point, the RF precoder in (20) is extended to multiple RF chains connection, and a digital precoder is needed in the system. Hence, the overall hybrid analog-digital precoder is given as

$$\mathbf{F} = \mathbf{F}_{\text{RF}}\mathbf{F}_{\text{BB}}, \quad (25)$$

  where $\mathbf{F}_{\text{BB}} \in \mathbb{C}^{N_{\text{RF}} \times U}$ is the digital baseband precoder and the size of $\mathbf{F}_{\text{RF}}$ is $M \times N_{\text{RF}}$ where each column in $\mathbf{F}_{\text{RF}}$ represents the precoder design of the signal at one RF chain controlled in the analog domain as given in (20). Note that the proposed precoding in this work should be applied here to control the design and compensate for the beam squint effect.
- In a sub-connected hybrid mMIMO designs [35], if the size of the sub-connected part of each RF chain experiences a remarkable amount of squinting, the proposed design must be implemented on each subarray. Otherwise, the given sub-connected part is implemented as conventional MIMO systems.

At this point, it should also be mentioned that the conventional digital precoder $\mathbf{F}_{\text{BB}}$ based on singular value decomposition for multi-RF LAS structure [28] can be implemented with the proposed design when multiple RF chains

are used. For example, a linear zero-forcing (ZF) precoder can be applied as a digital baseband precoder as $\mathbf{F}_{\text{BB}}^{\text{ZF}} = \mathbf{H}_{\text{eff}}^{H}(\mathbf{H}_{\text{eff}}\mathbf{H}_{\text{eff}}^{H})^{-1}$ where $\mathbf{H}_{\text{eff}} = \mathbf{H}\mathbf{F}_{\text{RF}}$ and $\mathbf{H}$ is the channel matrix. However, a hybrid precoder design that compensates for the effect of beam squinting at both digital and analog sides with the use of the proposed LAS analog transceiver structure is left for future work.

IV. System Analysis

In this section, the proposed design is analyzed in terms of capacity and power consumption.

A. Capacity

Once the beam squint effect is compensated, the lost beam gain is reclaimed, thus the capacity is improved toward the desired direction. With the proposed design, for a single RF chain, the capacity is given as

$$C_{\text{LAS}} = \sum_{k'=1}^{N_F} \frac{W_b}{N'} \sum_{k''=0}^{N'-1} \log_2 \left[1 + \frac{\gamma N'}{W_b} \left| g\left(\theta_{\text{LAS}}^{\text{opt}}(k'), f_{k''|_{k'}}\right)\right|^2 \right], \tag{26}$$

where $\theta_{\text{LAS}}^{\text{opt}}(k')$, $f_{k''|_{k'}}$ is the effective beam direction due to all lens elements for k'^{th} subband. $N' = W_b/\Delta f$ is the number of subcarriers within each subband, and $f_{k''|_{k'}}$ is the frequency of the k''^{th} subcarrier within k'^{th} subband. Here, it is important to reiterate that, $\theta_{\text{LAS}}^{\text{opt}}(k')$ for k'^{th} subband is obtained based on the subband's center frequency $f_{k'}$, thus other subcarriers at $f_{k''} \neq f_{k'}$ within the subband may still cause some residual squinting. This is taken care of during the design of N_F in (17) as discussed in Section III-A.

In order to compare the capacity of our proposed design with the capacity of (12) under beam squint effect, given that the ratio W_b/N' is fixed over all subbands which is equal to the ratio W/N in the conventional capacity formula, it is noticed that the capacity is mainly decided by the beam gain obtained in different physical directions at different subcarriers. This indicates that the beam gain loss caused by the beam squint effect is vital to the system capacity. Therefore, the capacity comparison can be simplified to beam gain comparison.

Based on (8) and (22), the ratio between the beam gain of the proposed design and the beam gain of the conventional mMIMO system under beam squinting effect at each subband frequency is given in (27), as shown at the bottom of the next page. where $\theta_{\text{opt}}^{(n)}$ belong to the optimum set $\Phi_{\text{opt}}(k') = \{\theta_{\text{opt}}^{(1)}, \theta_{\text{opt}}^{(2)}, \ldots, \theta_{\text{opt}}^{(n)}, \ldots, \theta_{\text{opt}}^{(N_L)}\}$ that gives $\theta_{\text{LAS}}^{\text{opt}}(k')$.

Since the proposed design depends on several factors to achieve the best performance such as the number of subband filters, number of lenses, and the desired direction, the beam ratio in (27) varies at each subband to be less or larger than one. Therefore, a careful design with an optimum number of subband filters and lenses needs to be taken into account to achieve the best capacity performance. This has been numerically analyzed in Fig. 14 in the numerical results Section. Additionally, the effect of changing the number of lenses is discussed in the next subsection.

B. Power Consumption

Due to the large antenna array structure in mMIMO systems, the power consumption of the circuits can account for a significant portion of the total system power consumption. Although the transmit power is the main consumer in the transmitter design, the power consumption of the circuits in each transmit antenna is also a non-negligible element in relation to the number of transmit antennas due to other analog devices such as digital-to-analog converter (DAC) as the main power consumers in the RF chain, PSs, and power amplifiers. The power consumption model of the conventional mMIMO system is analyzed in [28] and is given as

$$\mathcal{P}_c^{\text{TA}} = \underbrace{\frac{\mathcal{P}_{\text{tx}}}{\eta_{\text{TA}}\eta_{\text{PA}}}}_{\substack{\text{Effective Tx} \\ \text{power term, } \mathcal{P}^{\text{TA}}}} + \underbrace{N_{\text{RF}} M \mathcal{P}_{\text{PS}}}_{\text{PS network term}} + \underbrace{N_{\text{RF}}\mathcal{P}_{\text{RF}}}_{\text{RF term}}, \tag{28}$$

where $\mathcal{P}_{\text{tx}}$, η_{TA} and η_{PA} are the system's transmit power, array aperture efficiency and power amplifier's efficiency, respectively. For the conventional mMIMO, η_{TA} is usually assumed to be 90% [28]. $\mathcal{P}_{\text{PS}}$ and $\mathcal{P}_{\text{RF}}$ represent the amount of power consumed by a PS and an RF chain, respectively.

Similarly, the total power consumed by the proposed LAS design can be divided into four parts, given as

$$\mathcal{P}_c^{\text{LAS}} = \underbrace{\frac{\mathcal{P}_{\text{tx}}}{\eta_{\text{LAS}}\eta_{\text{PA}}\eta_{\text{SW}}\eta_{\text{filter}}}}_{\substack{\text{Effective Tx} \\ \text{power term, } \mathcal{P}^{\text{LAS}}}} + \underbrace{N_{\text{RF}} N_L \mathcal{P}_{\text{PS}}}_{\text{PS network term}} + \underbrace{N_{\text{RF}} N_L \mathcal{P}_{\text{SW}}}_{\substack{\text{switching network} \\ \text{term}}} + \underbrace{N_{\text{RF}}\mathcal{P}_{\text{RF}}}_{\text{RF term}}, \tag{29}$$

where η_{LAS}, $\eta_{\text{SW}} = 10^{-\text{IL}_{\text{SW}}/10}$ and $\eta_{\text{filter}} = 10^{-N_F \text{IL}_{\text{filter}}/10}$ are LAS aperture, switch, and subband filters power efficiency, respectively, with IL_{SW} and $\text{IL}_{\text{filter}}$ being insertion losses of the switch and the filter. The LAS aperture efficiency is generally assumed to be 80% due to lens/air mismatch [28].

In order to analyze the total power consumption by the conventional mMIMO and the proposed LAS design, we compare the corresponding terms in (28) and (29). Note that the power consumed by RF chains (i.e., the RF terms in (28) and (29)) are the same in both cases, thus, can be disregarded in the comparison. The effective power terms $\mathcal{P}^{\text{TA}}$ and $\mathcal{P}^{\text{LAS}}$ can be related by $\mathcal{P}^{\text{LAS}} = \mathcal{K}\mathcal{P}^{\text{TA}}$ where

$$\mathcal{K} = \frac{\eta_{\text{TA}}}{\eta_{\text{LAS}}\eta_{\text{SW}}\eta_{\text{filter}}}. \tag{30}$$

Since $\eta_{\text{LAS}} < \eta_{\text{TA}}$ and considering the extra insertion losses due to the filters and the switches, $\mathcal{K}$ is always greater than one which makes $\mathcal{P}^{\text{LAS}} > \mathcal{P}^{\text{TA}}$. This means that the LAS design requires more power to achieve the same effective isotropic radiated power as the conventional mMIMO design. Furthermore, the presence of switches (which are active circuitry elements) introduces an extra power consumption in the LAS design. Nevertheless, this extra power consumption in the LAS design is counteracted by a significant reduction in the number of PSs. The number of PSs in the LAS design is reduced by the factor of P (i.e., $M = N_L \times P$) which significantly reduces the PS term in (29) as compared to (28).

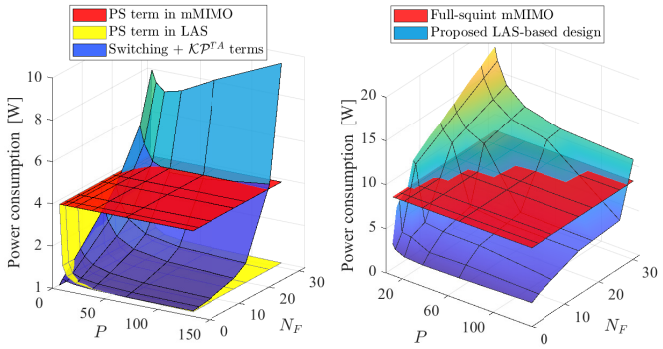

(a) Power consumption of each term (b) Total power consumption

Fig. 8. Power consumption vs P analysis. Here, both the conventional mMIMO and the proposed LAS-based designs follow the design parameters mentioned in Table I.

The power consumed by these individual terms is illustrated in Fig. 8a as a function of P and N_F. Apparently, the PS term in the conventional mMIMO is independent of both P and N_F while the PS term in the proposed design only depends on P. This is plausible since, for a given M, the number of PS ($= N_L$ for $N_L > 1$) required in the LAS design decreases as P increases. Therefore, increasing P leads to the reduction of the total power consumed by the PS term. As the extreme case where $P = M$, i.e., single-lens design in which PS network is no longer required,[2] the PS term vanishes from (29). For the switching and the effective power terms, their total power consumption varies with both P and N_F. For low N_F values the total power consumed by these two terms decreases as P increases. On the other hand, for high N_F values the total power varies convexly with P. Note that, with high N_F, the total power consumed by the proposed LAS design surpasses that of the conventional mMIMO, as shown by Fig. 8b. In order to ensure low power consumption in the proposed design, the choice of P and N_F need to be done carefully. Note that the choice of N_F is governed by (17). In order to facilitate power efficiency, the minimum N_F that satisfies (17) can be chosen. The choice of P which is more flexible can follow after choosing N_F. Note that, as it can be seen from Fig. 8b, although higher values of P are advantageous in terms of power consumption, it compromises the controllability of the beam squint effect through PS network due to the reduced number of lenses and PSs. On the other hand, lower values of P cause relatively high power consumption and it also leads to the loss of the beam squint controllability through the switching network. Therefore the best practice is to heuristically select a moderate value of P that facilitates both adequate controllability of the beam squint and low power consumption.

It is clear from the above analysis that the choice of P and N_F are critical for both beam squint controllability (which has a direct impact on the system capacity) and the total power consumption. Therefore, it is also pertinent to analyze the system's energy efficiency (EE) as a function of these two design parameters. The EE is generally defined as the ratio of the system capacity and its average power consumption, given as

$$EE = \frac{C_{\text{LAS}}}{\mathcal{P}_c^{\text{LAS}}}. \tag{31}$$

C. Practical Implementation

Since the proposed LAS architecture features some hardware design, it is important that we shed light on the practical feasibility and availability of the additional hardware components required to implement the architecture. In fact, there has been some immense effort invested in realizing the practical implementation of LAS systems similar to the one exploited in this work. For instance, the works of Mumcu et al. in [36] and [37] have developed some prototypes of LAS architectures with 1D and 2D lenses, respectively, and provided detailed design steps. Apparently, the practical realization of the modified LAS architecture proposed in our work may follow similar design steps only with the insertion of the subband filter as an extra design step.

It is also important to highlight that, for the proper functioning of the proposed architecture, the required narrowband filters should be of high quality and operate at high-frequency bands. In the current state-of-the-art, such filters are bulky and expensive. However, there has been active research on the realization of such filters based on Surface Acoustic Wave (SAW) and Bulk Acoustic Wave (BAW) technologies, which is expected to address both the bulkiness and cost issues [38].

Furthermore, as we have pointed out in Section III-A, our proposed LAS architecture replaces the SPMT switches in the traditional LAS with MPMT switches. Both SPMT and MPMT switch configurations have been widely studied and adopted in various practical systems [39], [40]. However, the limited number of poles in most of the commercially available MPMT switches may pose some difficulty in the realization of the proposed system, especially when a number of subbands N_F is huge. Nevertheless, higher-order MPMT switching configurations can also be achieved by using multiple SPMT switches arranged serially. High quality SPMT switches operating in a wide range of frequencies are widely available on the market at very low cost [41].

V. Numerical Results and Discussion

In this section, we analyze the performance of the proposed precoder design in terms of beam gain, complexity, and overall

[2]In the LAS design, PS network is responsible for connecting the lenses by introducing the delays to the signal passed to each lens. As such, in the case of a single lens system, PS network is no longer required.

$$\frac{g(\theta_{\text{LAS}}^{\text{opt}}(k'), f_{k'})}{g^{(\text{BS})}(\hat{\theta}, f_{k'})} = \frac{\frac{1}{\sqrt{N_L P}} \sum_{n=0}^{N_L-1} \sum_{p=0}^{P-1} e^{-j2\pi \frac{d}{c}(Pn+p)(f_{k'}+f_c)\sin\theta_{\text{LAS}}^{\text{opt}}(k')} e^{-j2\pi \frac{d}{c} f_c Pn \sin\hat{\theta}} e^{-j2\pi \frac{d}{c} f_c (\frac{(P-1)}{2}-p)\sin\theta_{\text{opt}}^{(n)}}}{\frac{1}{\sqrt{M}} \sum_{m=1}^{M} e^{-j2\pi \frac{d}{c}(m-1)\left[(f_{k'}+f_c)\sin\hat{\theta} - f_c \sin\hat{\theta}\right]}}. \tag{27}$$

TABLE I
SIMULATION PARAMETERS

Parameters	Value
Operating frequency f_c	60 GHz
System bandwidth W	5 GHz
Channel paths L_p	1
Antenna elements M	128
Distance between antenna elements d	$\lambda_c/2$
Number of RF chains N_{RF}	1
Number of subcarrier frequencies N	2048
Number of lenses N_L	4
Number of analog subband filters N_F	16
Number of antenna per lens P	M/N_L
Desired direction $\hat{\theta}$	$\pi/4$
Power efficiency of amplifier η_{PA}	0.2 [28]
Insertion loss of filter $\text{IL}_{\text{filter}}$	1 dB
Power consumption of PS P_{PS}	30 mW [28]
Power consumption of one RF chain P_{RF}	220 mW [28]

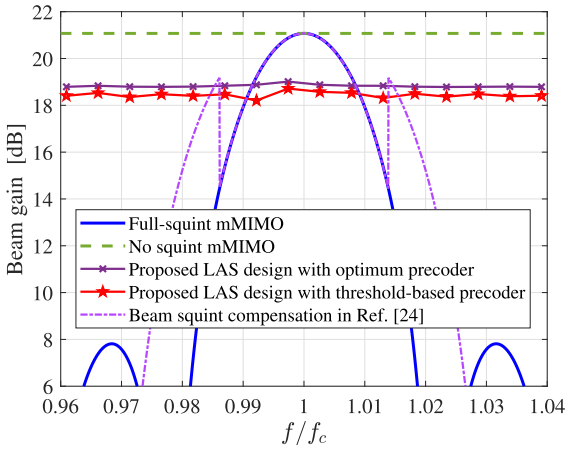

Fig. 9. Beam gain vs normalized frequency.

system capacity. Afterward, considering the inclusion of some extra hardware components in the proposed architecture which may increase the system's power consumption, we delve into the detailed examination of the system's energy efficiency. Subsequently, we analyze the impact of parameter selection on the overall system performance, aiming at understanding the nuances and trade-offs involved in choosing specific design parameters. Finally, we extend our analysis to the multiuser case, exploring how the proposed design adapts and performs in a scenario involving multiple users. This comprehensive analysis aims to provide a holistic understanding of the proposed precoder design across various performance metrics and operational scenarios.

Unless stated otherwise, we use the numerical values of the system parameters from Table I in this analysis. We benchmark the performance of the proposed LAS-based design against two configurations of conventional mMIMO systems: one considering the full beam squint effect, denoted as "Full-squint mMIMO," and the other disregarding beam squint effect (i.e., the ideal case), referred to as "No squint mMIMO." Additionally, we compare the performance of the proposed design with existing state-of-the-art solutions, including the designs presented in [15], [16], and [24]. To ensure a fair and meaningful comparison, we align the parameters used in [15], [16], and [24] with those detailed in Table I. It's important to note that the power consumption model for [24] follows (29), excluding the terms related to switching. For a single-user scenario, we adopt the array vector of a single subcarrier approach from [15] for the analog precoding design, while mean channel matrix (MCM) and mean channel covariance matrix (MCCM)-based digital precoding approaches are adopted for both single-user and multi-user scenarios. This thorough comparative analysis aims to provide a rigorous understanding of the proposed LAS-based design's performance with conventional mMIMO systems and other contemporary beam squint solutions. It ensures a fair and insightful assessment across various precoding strategies.

A. Proposed Precoder Design Performance

Here, we evaluate the performance of our proposed precoder design in terms of beam gain, complexity, and capacity.

In beam gain evaluation, the achievable beam gain with the proposed LAS-based design is given in Fig. 9, benchmarked with "Full-squint mMIMO" and "No squint mMIMO" as well as with [24]. The beam gain provided by the proposed design is analyzed with both the full exhaustive search and the proposed threshold-based search approach. While both cases significantly improve the gain (to less than $\approx$ 3 dB of ideal performance), the exhaustive search, as expected, performs relatively better, though at the expense of high complexity, as analyzed in Fig. 10. However, due to the loss introduced by lens structure as discussed in [28], the beam gain of the proposed design can not reach the performance of an ideal mMIMO system (with no squinting). Note that the proposed design achieves significant gain enhancement compared to the design presented in [24] as the deviation of the subcarrier frequency from f_c increases. The rationale behind this behavior is due to the frequency-dependent property of the analog precoder introduced in the proposed analog LAS design. Unlike the work of [24] where each subband filter and its associated PS perform the beam squint correction with respect to the center frequency of that filter only which limits the achievable beam gain performance, especially for the edge subbands, the analog precoder in our proposed design corrects the beam squint pertained to each subband with respect to the system's carrier frequency f_c.

The exhaustive search-based precoder complexity is calculated as the total number of possible beam sets in the system for a given subband. The precoder needs to search over all possible sets and choose the set that has the minimum beam deviation that fulfills the condition (23). On the other hand, the proposed threshold-based method determines the precoder complexity by counting the number of beam sets that are examined to achieve the optimal set that reduces the beam deviation to a specific threshold value that satisfies the condition (24). Fig. 10 shows a huge difference in complexity between the exhaustive search (which is in the order of millions) and the proposed threshold-based precoder (only hundreds to few thousand) at each subband. This is due to the simplified searching mechanism adopted by the proposed precoder, as explained in Section III-B.

Figure 11 illustrates the capacity versus bandwidth performance of the proposed LAS design in comparison to

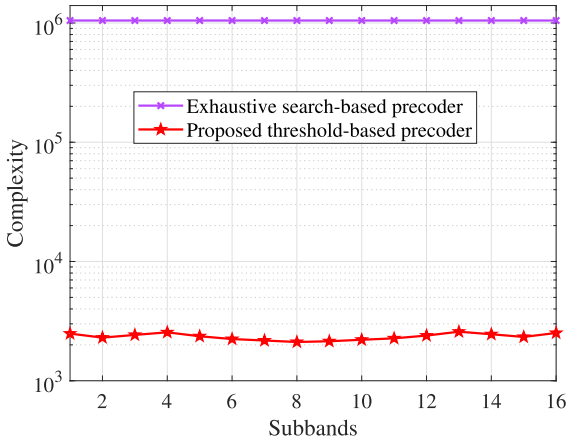

Fig. 10. Complexity analysis.

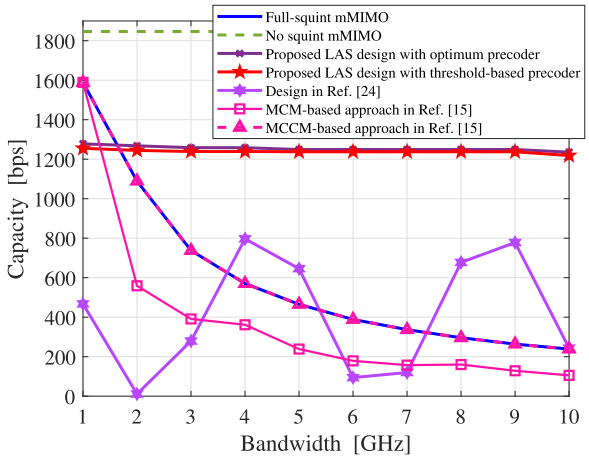

Fig. 11. Capacity vs bandwidth analysis.

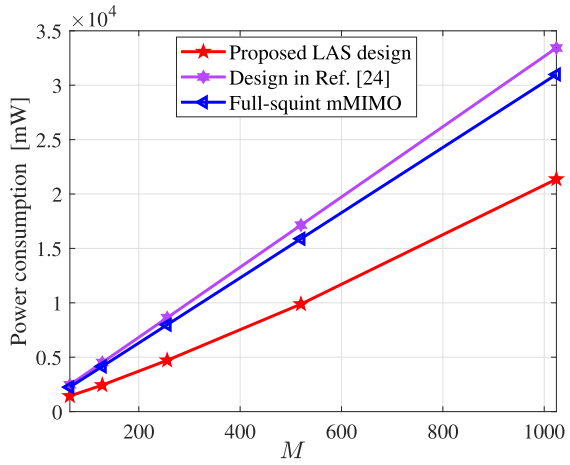

Fig. 12. Power consumption vs M analysis.

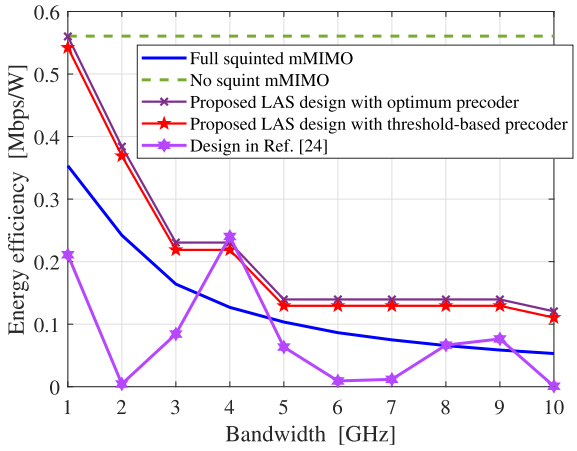

Fig. 13. Energy efficiency vs bandwidth analysis.

the contemporary designs presented in [15] and [24] under 10 dB SNR. Notably, our proposed design maintains a stable and superior capacity performance for different bandwidths, whereas the design in [15] and [24] experience high capacity degradation as bandwidth increases. Furthermore, the capacity performance of [24] oscillates as the bandwidth increases due to the inherent number of filters in the design.

B. Energy Efficiency Performance

In this subsection, we analyze the power consumption and energy efficiency of the proposed LAS design compared to other related designs in the literature (i.e., the design in [24]).

In practice, since the values of P_{SW} are only available for the few ports MPMT switches, we model the N_F-poles $\times$ P-throws MPMT switch considered in our design as a series of SP2T switches for each pole for power consumption analysis. Therefore, the term P_{SW} in (29) becomes $\log_2(P)N_F P_{\text{SW}}^{(s)}$, where $P_{\text{SW}}^{(s)} = 10$ mW is the power consumption of an SP2T switch, while $\text{IL}_{\text{SW}} = \log_2(P) \times 1$ dB [28]. The calculated power consumption for different array sizes is summarized in Fig. 12. The performance is compared with that of the conventional mMIMO system (i.e., (28)), and with [24] which also presents subband-based beam squinting compensation design. It is clear from Fig. 12 that the proposed LAS design is the most power-efficient design while profitably compensating for the beam squinting, which makes it suitable for commercial applications of mMIMO networks.

In Fig. 13, the energy efficiency performance of the proposed LAS design across various bandwidths is illustrated. It is compared with the design presented in [24] under a SNR of 10 dB. In particular, it is observed that while the performance of the proposed design experiences a decline with an increase in system bandwidth, it consistently outperforms existing approaches. The proposed LAS design demonstrates superior energy efficiency compared to UWB mMIMO systems without squint compensation, even in scenarios with elevated bandwidths. This observation underscores the effectiveness of the proposed LAS design in achieving commendable energy efficiency across a spectrum of bandwidths, positioning it as a competitive solution compared to existing approaches.

C. Impact of the Design Parameters Selection

In this subsection, we turn our attention to examining the influence of varying hardware parameters on the proposed design's performance, specifically assessing their impact on system capacity and energy efficiency. The parameters under scrutiny include the transmit direction $\hat{\theta}$, the number of subband filters N_F, and the number of lenses N_L incorporated in the design. This systematic analysis aims to elucidate the sensitivity of the proposed design to alterations in these

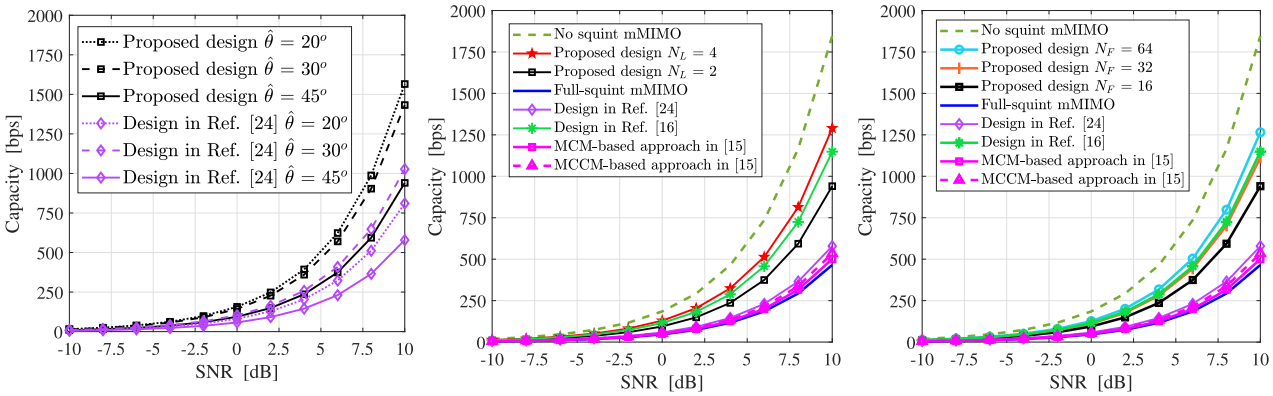

(a) $N_F = 16$, $N_L = 2$, different angles (b) $N_F = 16$, $\hat{\theta} = \pi/4$, different N_L (c) $N_L = 2$, $\hat{\theta} = \pi/4$, different N_F

Fig. 14. Capacity vs SNR analysis in a single user scenario.

crucial hardware parameters, providing valuable insights into the trade-offs and considerations associated with different parameter choices.

Fig. 14 gives some insights regarding the effects of the design parameters $\hat{\theta}$, N_F, and N_L on the system capacity of the proposed design for a point-to-point link scenario with a single-antenna receiver. The system performance here is compared with the performances of the designs presented in [16] and [24]. Since the beam squinting amount suffered by the system is a function of the desired direction $\hat{\theta}$ and increases as $\hat{\theta}$ deviates further from the array's boresight (see Figs. 2a—2c), the proposed design in section III-A considers the worst case which is $\hat{\theta}_{\max} = \pi/4$ for LAS systems [28]. Fig. 14(a) analyzes the capacity performance of the proposed design for different $\hat{\theta}$ ($\leq \hat{\theta}_{\max}$). Clearly, the system capacity performance improves for all $\hat{\theta}$ ($<\leq \hat{\theta}_{\max}$). This implies that, with the proposed approach, the system can be designed once, based on the worst-case scenario, and work for all other scenarios without the need for changing the design parameters. It is also clear from the figure that the proposed design outperforms that of [24] for different $\hat{\theta}$. In Fig. 14(b), we only analyze the proposed design when both steering mechanisms, i.e., PS and switching networks, have a notable effect in controlling the beam squint amount. The figure shows that there is capacity gain as the number of lenses (i.e., N_L) is increased. We reckon that this improvement comes from increasing the number of individual beams that are responsible for providing the resultant beam while keeping the switching network dominant over the PS network which in return enhances the controllability of beam squint amount.

Likewise, increasing the number of filters N_F improves system capacity as shown in Fig. 14(c). With the same W, larger N_F means reducing the subband sizes which in turn reduces the residual squint effect within each subband (refer to (14) in section III-A). However, since increasing N_F also elevates the system's energy consumption, it is imperative to weigh the achieved capacity gain against the energy efficiency as a function of N_F. This analysis is presented in Fig. 15. While it is clear that the capacity enhancement through increasing N_F comes at the expense of degraded energy efficiency, the proposed design still outperforms the conventional system in terms of both capacity and energy efficiency for a wide

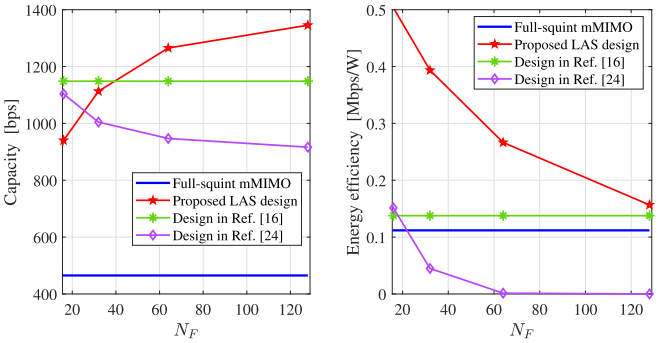

(a) (b)

Fig. 15. (a) Capacity and (b) energy efficiency vs number of subband filters N_F analysis.

range of N_F values. It is also clear from the figure that, although (17) gives wide flexibility on the choice of N_F, the best choice remains to be the minimum N_F that satisfies (17) when system's energy efficiency is of great concern.

D. Performance In Multiuser Case

Expanding the applicability of our proposed approach to multiuser networks, this section undertakes an evaluation of system capacity within scenarios involving multiple users. In this context, the proposed LAS design is assumed to be assessed utilizing a threshold-based precoder approach, incorporating the use of ZF precoder in its digital baseband domain.

The system capacity vs SNR is analyzed in Fig. 16 for 10 users (i.e., $U = N_{\text{RF}} = 10$) and compared with the precoding design presented in [15] and [16]. The performance is also compared with the full-squint mMIMO system capacity with an SVD-based approach. The system capacity for the proposed LAS design is given as

$$C_{\text{LAS}} = \sum_{k'=1}^{N_F} \frac{W_b}{N'} \sum_{k''=0}^{N'-1} \log_2 \left(\left| \mathbf{I}_{N_{\text{RF}}} + \frac{\gamma N'}{W_b} \times \left(\mathbf{H}(k'') \mathbf{F}_{\text{RF}}(k') \mathbf{F}_{\text{BB}}(k'') \mathbf{F}_{\text{BB}}^*(k) \mathbf{F}_{\text{RF}}^*(k') \mathbf{H}^*(k'') \right) \right| \right). \tag{32}$$

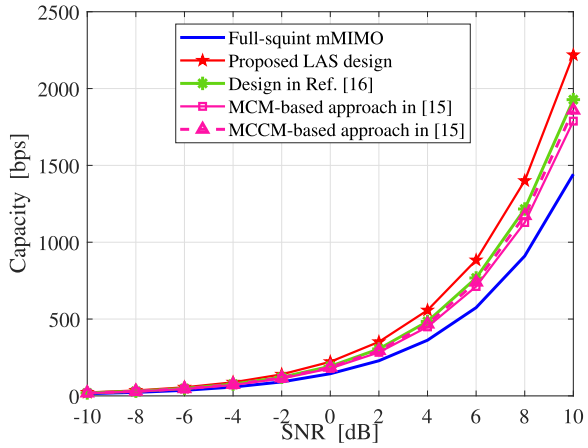

Fig. 16. Capacity vs SNR analysis in multi-user scenario.

Our proposed analog LAS transceiver design has demonstrated superior performance compared to alternative methods and designs discussed in the existing literature. This outcome substantiates the effectiveness of our proposed design in successfully mitigating the beam squint effect in a multi-user environment.

VI. Conclusion and Future Directions

In this work, we introduce a novel analog transceiver design leveraging the LAS architecture and subband filters to mitigate the beam squint effect in UWB mMIMO systems. The proposed design exhibits effectiveness with both traditional exhaustive search-based precoding and a simpler threshold-based precoding technique. Simulation results confirm the robust system performance of the proposed LAS-based transceiver design under both precoding strategies. While the proposed design is implementable with off-the-shelf components, optimal performance recommends the use of high-quality narrowband filters, particularly in higher frequency bands, an area currently under research [38]. The extension of this design to multi-user scenarios employing a 2D antenna array and hybrid precoding for reduced beam squinting effects in both analog and digital domains is deferred for future exploration. Furthermore, the proposed design can also be extended to the near-field communication scenario. In this case, the severity of beam squint is a function of not only direction and frequency but also distance. Optimization of the proposed design to fit in the near-field scenario is also left for future work.

References

[1] J. Brady and A. Sayeed, "Wideband communication with high-dimensional arrays: New results and transceiver architectures," in *Proc. IEEE Int. Conf. Commun. Workshop*, London, U.K., Jun. 2015, pp. 1042–1047.

[2] M. Wang, F. Gao, S. Jin, and H. Lin, "An overview of enhanced massive MIMO with array signal processing techniques," *IEEE J. Sel. Topics Signal Process.*, vol. 13, no. 5, pp. 886–901, Sep. 2019.

[3] S. A. Busari, K. M. S. Huq, S. Mumtaz, L. Dai, and J. Rodriguez, "Millimeter-wave massive MIMO communication for future wireless systems: A survey," *IEEE Commun. Surveys Tuts.*, vol. 20, no. 2, pp. 836–869, 2nd Quart., 2018.

[4] D. Cassioli, M. Z. Win, and A. F. Molisch, "The ultra-wide bandwidth indoor channel: From statistical model to simulations," *IEEE J. Sel. Areas Commun.*, vol. 20, no. 6, pp. 1247–1257, Aug. 2002.

[5] F. Liu, C. Masouros, A. P. Petropulu, H. Griffiths, and L. Hanzo, "Joint radar and communication design: Applications, state-of-the-art, and the road ahead," *IEEE Trans. Commun.*, vol. 68, no. 6, pp. 3834–3862, Jun. 2020.

[6] B. Wang, F. Gao, S. Jin, H. Lin, and G. Y. Li, "Spatial-and frequency-wideband effects in millimeter-wave massive MIMO systems," *IEEE Trans. Signal Process.*, vol. 66, no. 13, pp. 3393–3406, Jul. 2018.

[7] B. Wang et al., "Spatial-wideband effect in massive MIMO with application in mmWave systems," *IEEE Commun. Mag.*, vol. 56, no. 12, pp. 134–141, Dec. 2018.

[8] D. B. Hunter, M. E. Parker, and J. L. Dexter, "Demonstration of a continuously variable true-time delay beamformer using a multichannel chirped fiber grating," *IEEE Trans. Microw. Theory Techn.*, vol. 54, no. 2, pp. 861–867, Feb. 2006.

[9] S. K. Garakoui, E. A. M. Klumperink, B. Nauta, and F. E. van Vliet, "Phased-array antenna beam squinting related to frequency dependency of delay circuits," in *Proc. 41th Eur. Microw. Conf.*, Manchester, U.K., Oct. 2011, pp. 1304–1307.

[10] M. Longbrake, "True time-delay beamsteering for radar," in *Proc. IEEE Nat. Aerosp. Electron. Conf. (NAECON)*, Dayton, OH, USA, Jul. 2012, pp. 246–249.

[11] O. Longman, G. Solodky, and I. Bilik, "Beam squint correction for phased array antennas using the tansec waveform," in *Proc. IEEE Int. Radar Conf. (RADAR)*, Washington, DC, USA, Apr. 2020, pp. 489–493.

[12] G. Li, H. Zhao, and H. Hui, "Beam squint compensation for hybrid precoding in millimetre-wave communication systems," *Electron. Lett.*, vol. 54, no. 14, pp. 905–907, Jul. 2018.

[13] I. Laurinavicius, H. Zhu, J. Wang, and Y. Pan, "Beam squint exploitation for linear phased arrays in a mmWave multi-carrier system," in *Proc. IEEE Global Commun. Conf. (GLOBECOM)*, Waikoloa, HI, USA, Dec. 2019, pp. 1–6.

[14] B. Wang, M. Jian, F. Gao, G. Y. Li, and H. Lin, "Beam squint and channel estimation for wideband mmWave massive MIMO-OFDM systems," *IEEE Trans. Signal Process.*, vol. 67, no. 23, pp. 5893–5908, Dec. 2019.

[15] Y. Chen, Y. Xiong, D. Chen, T. Jiang, S. X. Ng, and L. Hanzo, "Hybrid precoding for wideband millimeter wave MIMO systems in the face of beam squint," *IEEE Trans. Wireless Commun.*, vol. 20, no. 3, pp. 1847–1860, Mar. 2021.

[16] R. Zhang, W. Hao, G. Sun, and S. Yang, "Hybrid precoding design for wideband THz massive MIMO-OFDM systems with beam squint," *IEEE Syst. J.*, vol. 15, no. 3, pp. 3925–3928, Sep. 2021.

[17] K. Dovelos, M. Matthaiou, H. Q. Ngo, and B. Bellalta, "Channel estimation and hybrid combining for wideband terahertz massive MIMO systems," *IEEE J. Sel. Areas Commun.*, vol. 39, no. 6, pp. 1604–1620, Jun. 2021.

[18] L. You et al., "Beam squint-aware integrated sensing and communications for hybrid massive MIMO LEO satellite systems," *IEEE J. Sel. Areas Commun.*, vol. 40, no. 10, pp. 2994–3009, Oct. 2022.

[19] Y. Chen, D. Chen, T. Jiang, and L. Hanzo, "Channel-covariance and angle-of-departure aided hybrid precoding for wideband multiuser millimeter wave MIMO systems," *IEEE Trans. Commun.*, vol. 67, no. 12, pp. 8315–8328, Dec. 2019.

[20] M. Cai et al., "Effect of wideband beam squint on codebook design in phased-array wireless systems," in *Proc. IEEE Global Commun. Conf. (GLOBECOM)*, Washington, DC, USA, Dec. 2016, pp. 1–6.

[21] H. Yu, P. Guan, Y. Wang, and Y. Zhao, "Performance analysis and codebook design for mmWave beamforming system with beam squint," *IEEE Wireless Commun. Lett.*, vol. 10, no. 9, pp. 2013–2016, Sep. 2021.

[22] X. Liu and D. Qiao, "Space-time block coding-based beamforming for beam squint compensation," *IEEE Wireless Commun. Lett.*, vol. 8, no. 1, pp. 241–244, Feb. 2019.

[23] B. Liu and H. Zhu, "Rotman lens-based two-tier hybrid beamforming for wideband mmWave MIMO-OFDM system with beam squint," *EURASIP J. Wireless Commun. Netw.*, vol. 2018, no. 1, pp. 1–13, Dec. 2018.

[24] Z. Sattar, J. V. C. Evangelista, G. Kaddoum, and N. Batani, "Antenna array gain and capacity improvements of ultra-wideband millimeter wave systems using a novel analog architecture design," *IEEE Wireless Commun. Lett.*, vol. 9, no. 3, pp. 289–293, Mar. 2020.

[25] F. Gao, B. Wang, C. Xing, J. An, and G. Y. Li, "Wideband beamforming for hybrid massive MIMO terahertz communications," *IEEE J. Sel. Areas Commun.*, vol. 39, no. 6, pp. 1725–1740, Jun. 2021.

[26] D. Qua Nguyen and T. Kim, "Joint delay and phase precoding under true-time delay constraints for THz massive MIMO," in *Proc. IEEE Int. Conf. Commun.*, Seoul, South Korea, May 2022, pp. 3496–3501.
[27] Z. Liu, W. ur Rehman, X. Xu, and X. Tao, "Minimize beam squint solutions for 60 GHz millimeter-wave communication system," in *Proc. IEEE 78th Veh. Tech. Conf. (VTC)*, Las Vegas, NV, USA, Sep. 2013, pp. 1–5.
[28] M. Karabacak, H. Arslan, and G. Mumcu, "Lens antenna subarrays in mmWave hybrid MIMO systems," *IEEE Access*, vol. 8, pp. 216634–216644, 2020.
[29] M. Karabacak, G. Mumcu, and H. Arslan, "Hybrid MIMO architecture using lens arrays," U.S. Patent 10 714 836, Jul. 14, 2020.
[30] L. Afeef, A. B. Kihero, and H. Arslan, "Novel transceiver design in wideband massive MIMO for beam squint minimization," 2022, *arXiv:2207.04679*.
[31] A. B. Kihero, L. Afeef, and H. Arslan, "Beam squint inspired multiple access technique in massive MIMO systems," in *Proc. IEEE 96th Veh. Technol. Conf. (VTC-Fall)*, London, U.K., Sep. 2022, pp. 1–6.
[32] Z. Wang, L. Cheng, J. Wang, and G. Yue, "Digital compensation wideband analog beamforming for millimeter-wave communication," in *Proc. IEEE 87th Veh. Technol. Conf. (VTC Spring)*, Porto, Portugal, Jun. 2018, pp. 1–5.
[33] S. Bhattacharyya and G. Aruna, "Radiation pattern analysis of uniform rectangular planar arrays for millimeter wave communications: Comparative study with uniform linear arrays," *Wireless Pers. Commun.*, vol. 112, no. 2, pp. 827–848, May 2020.
[34] O. E. Ayach, S. Rajagopal, S. Abu-Surra, Z. Pi, and R. W. Heath, "Spatially sparse precoding in millimeter wave MIMO systems," *IEEE Trans. Wireless Commun.*, vol. 13, no. 3, pp. 1499–1513, Mar. 2014.
[35] S. Han, I. Chih-Lin, Z. Xu, and C. Rowell, "Large-scale antenna systems with hybrid analog and digital beamforming for millimeter wave 5G," *IEEE Commun. Mag.*, vol. 53, no. 1, pp. 186–194, Jan. 2015.
[36] G. Mumcu, M. Kacar, and J. Mendoza, "Mm-wave beam steering antenna with reduced hardware complexity using lens antenna subarrays," *IEEE Antennas Wireless Propag. Lett.*, vol. 17, no. 9, pp. 1603–1607, Sep. 2018.
[37] K. A. Shila and G. Mumcu, "A millimeter-wave 2D beam steering antenna using extended hemispherical dielectric lens antenna subarrays," *IEEE Access*, vol. 10, pp. 103065–103073, 2022.
[38] *Greensboro, Advanced BAW Filter Technology and Its Impact on 5G*, Qorvo, Greensboro, NC, USA, 2020.
[39] W. Lee and S. Hong, "Low-loss and small-size 28 GHz CMOS SPDT switches using switched inductor," in *Proc. IEEE Radio Freq. Integr. Circuits Symp. (RFIC)*, Philadelphia, PA, USA, Jun. 2018, pp. 148–151.
[40] T. N. Msimango and V. M. Srivastava, "Fabrication and testing of double-pole four-throw switch with n-MOSFETs," *J. Eng. Sci. Technol.*, vol. 14, no. 6, pp. 3457–3469, 2019.
[41] Q. Xiao, G. Samiotes, T. Galluccio, and B. Rizzi, "A high performance DC-20 GHz SPDT switch in a low cost plastic QFN package," in *Proc. Eur. Microw. Conf. (EuMC)*, Rome, Italy, Sep. 2009, pp. 1673–1676.

Liza Afeef received the B.S. degree in communication technology engineering from Al-Balqa Applied University, Jordan, in 2014, and the M.S. degree in electrical engineering/wireless communication from Jordan University of Science and Technology (JUST), Jordan, in 2018. She is currently pursuing the Ph.D. degree with Istanbul Medipol University, Turkey. She is also a Research Assistant with the Communication, Signal Processing and Networking Center (CoSiNC). Her research interests include beamforming, massive and XL-MIMO, near-field and far-field propagation, beam management, MIMO channel modeling and exploitation, lens antenna, and physical layer authentication for next-generation wireless systems.

Abuu B. Kihero received the B.S. degree in electronics engineering from Gebze Technical University, Turkey, in 2015, and the M.S. degree in electrical, electronics, and cyber systems from Istanbul Medipol University, Istanbul, Turkey, in 2018, where he is currently pursuing the Ph.D. degree in wireless communication technologies. He is also a Research Assistant with the Communication, Signal Processing, and Networking Center (CoSiNC), Istanbul Medipol University. His research interests include wireless channel modeling and emulation, massive MIMO and extra-large MIMO techniques, interference modeling, synchronization techniques for coordinated multipoint (CoMP) networks, and physical layer security for 5G and beyond wireless systems.

Hüseyin Arslan (Fellow, IEEE) received the B.S. degree from Middle East Technical University (METU), Ankara, Turkey, in 1992, and the M.S. and Ph.D. degrees from Southern Methodist University (SMU), Dallas, TX, USA, in 1994 and 1998, respectively.

From January 1998 to August 2002, he was with the Research Group, Ericsson, where he was involved with several projects related to 2G and 3G wireless communication systems. Since August 2002, he has been with the Electrical Engineering Department, University of South Florida, where he was a Professor. In December 2013, he joined Istanbul Medipol University to found the Engineering College, where he is currently the Dean and a Professor of the School of Engineering and Natural Sciences. In addition, he was a part-time Consultant for various companies and institutions, including Anritsu Company and The Scientific and Technological Research Council of Turkey. He conducts research in wireless systems, with an emphasis on the physical and medium access layers of communications. His current research interests include 5G and beyond radio access technologies, physical layer security, interference management (avoidance, awareness, and cancellation), cognitive radio, multi-carrier wireless technologies (beyond OFDM), dynamic spectrum access, co-existence issues, non-terrestrial communications (high altitude platforms), joint radar (sensing), and communication designs. He has been collaborating extensively with key national and international industrial partners and his research has generated significant interest in companies, such as InterDigital, Anritsu, NTT DoCoMo, Raytheon, Honeywell, and Keysight Technologies. Collaborations and feedback from industry partners have significantly influenced his research. In addition to his research activities, he also contributed to wireless communication education. He has integrated the outcomes of his research into education which led him to develop a number of courses at the University of South Florida. He has developed a unique "wireless systems laboratory" course (funded by the National Science Foundation and Keysight Technologies) where he was able to teach not only the theory but also the practical aspects of wireless communication systems with the most contemporary test and measurement equipment.

Dr. Arslan served as the general chair, the technical program committee chair, the session and symposium organizer, the workshop chair, and a technical program committee member for several IEEE conferences. He is currently a member of the Editorial Board of the IEEE COMMUNICATIONS SURVEYS AND TUTORIALS and the IEEE SENSORS JOURNAL. He served as a member of the Editorial Board for IEEE TRANSACTIONS ON COMMUNICATIONS, IEEE TRANSACTIONS ON COGNITIVE COMMUNICATIONS AND NETWORKING, and several other scholarly journals by Elsevier, Hindawi, and Wiley Publishing.